NUMERICAL INVESTIGATION OF ROD VORTEX GENERATORS ON HOVERING HELICOPTER ROTOR BLADES

FERNANDO TEJERO EMBUENA, PIOTR DOERFFER, PAWEŁ FLASZYŃSKI, OSKAR SZULC

The Szewalski Institute of Fluid-Flow Machinery
Polish Academy of Sciences
Fiszera 14, 80-231 Gdańsk, Poland
email: fernando.tejero@imp.gda.pl, www.imp.gda.pl

Key Words: *Helicopter Rotor, Hover, Shock Wave, Flow Separation, Vortex Generator, Flow Control*

Abstract. The paper presents the possible application of a passive flow control device on helicopter rotor blades. Recently, own invention of a rod vortex generator (RVG) has been investigated in a curved wall nozzle [2] and its application to helicopters is analyzed in this article. The validation of the numerical model for the clean case is based on the Caradonna and Tung model helicopter rotor. For the studied flow conditions, a strong shock wave located close to the tip induces flow separation. The proposed passive flow control system is able to reattach the flow to the wall improving the aerodynamic performance of the rotor.

1 INTRODUCTION

Interest in flow control systems such as synthetic jets or vortex generators and its application for separation control is rising in the last years. Recently, own invention of a passive streamwise vortex generator (rod vortex generator – RVG [1]) has been studied in a curved channel within the framework of the UFAST project [2] (Unsteady Effects of Shock Wave Induced Separation, 2005-2009). RVGs are submerged in the boundary layer which provides the best compromise between the effectiveness in reducing the separation and device-drag. The basic flow control mechanism is based on the intensification of exchange of momentum in the direction normal to the wall. High momentum air is transferred to the low momentum region close to the surface and therefore the separation bubble is reduced. Rod vortex generators are defined by 5 parameters: diameter (ϕ), height (h), spacing (L), skew angle (α) and pitch angle (Θ) (see fig. 1). The first three values are proportional to the boundary layer thickness while skew and pitch angles are optimized for inducing the strongest streamwise vortex. A deployment of a single rod vortex generator induces a strong streamwise vorticity due to the interaction between the mean flow and the rod (see fig.2).

As a step forward the research is focused on the application of the device to complex geometries. This paper studies the proposed flow control system in terms of the improvement of aerodynamic performance of hovering rotor blades.
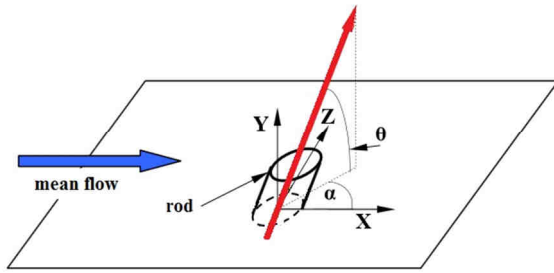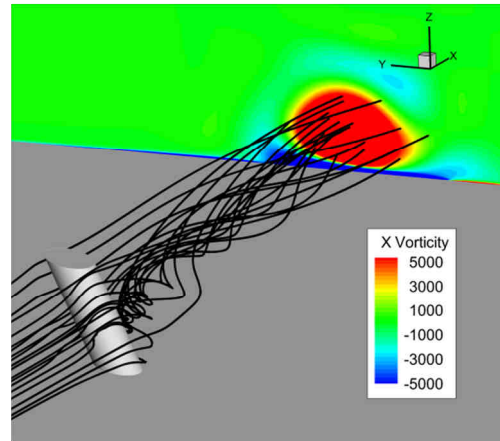
Figure 1: RVG schematic view

Figure 2: Isolated RVG inducing streamwise vortex

2 CARADONNA AND TUNG EXPERIMANTAL SET-UP

The CFD validation of the FLOWer solver [3] for the clean case is performed against the experimental data of Caradonna and Tung [4]. This experimental database is extensively used for verification of CFD codes in rotorcraft applications. The data was gathered in the Army Aeromechanics Laboratory's hover test facility in the 80's. The model employed two cantilever-mounted, rectangular, untwisted and untapered NACA0012 rigid blades. The radius (R) of the rotor was 3.75 ft (1.143 m) with a chord (c) equal to 0.625 ft (0.1905 m) which leads to an aspect ratio of 6.0 (see fig. 3). Different rotational speeds of the rotor were
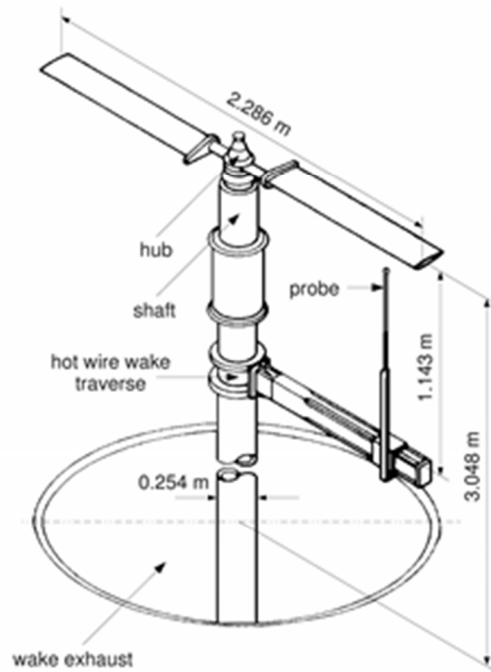

Figure 3: Experimental set-up of the Caradonna-Tung two-bladed model rotor in hover [4]

applied during the experiments (650-2540 RPM) which varied the tip Mach number from 0.226 to 0.890. Moreover, the collective pitch was set in the range of 0˚ - 12˚. Pressure distribution was measured at five cross-sections along the blade and the tip vortex trajectory was acquired with a hot-wire probe mounted beneath the rotor.

3 FLOWER SOLVER FROM DLR

The present CFD investigation was carried out with the FLOWer solver from DLR which solves the Favre-averaged Navier-Stokes equations with different turbulence models. The chimera overlapping grids technique [5] is implemented in the code to model complex geometries. The Linear Explicit Algebraic Stress model (LEA k-ω [6]) was used for the numerical investigation due to improved prediction capabilities for transonic flows. The numerical algorithm is based on a semi-discrete approach with a finite-volume, central scheme and 2nd order of accuracy for the spatial discretization and an explicit Runge-Kutta method for integration in time (CFL number of 2.5).

4 NUMERICAL RESULTS: CLEAN CASE AND FLOW CONTROL CASE

4.1 Clean case

The authors of the paper have been dealing with the numerical simulation of the Caradonna and Tung model helicopter rotor blade in high-speed hover in the past. The complex flow around the blades was simulated using different physical models (steady, unsteady), numerical grids (block-structured, chimera), flow solvers (SPARC, FLOWer and NUMECA) and turbulence models (i.e. Spalart-Allmaras) with success [7, 8, 9].

For validation of the two-equations LEA k-ω turbulence model implemented in FLOWer, a transonic test-case with a tip Mach number of $M_T = 0.877$, tip Reynolds number equal to $Re_T = 3.93 \cdot 10^6$ and collective pitch of $\Theta_c = 8˚$ has been chosen.

For the numerical investigation, the computational domain is formed by a cylindrical background grid and 2 blade grids in chimera set-up. Two "hole" meshes are added to the domain which are used to blank unnecessary cells of the grid components (needed for the chimera interpolation procedure). The complete set of meshes consists of 114 blocks and 12.70 millions of control volumes. Table 1 summarizes the different chimera overlapping grid components, number of blocks and control volumes of the computational mesh.

Table 1: Grid components for the clean case.

grid component	number of blocks	number of volumes
background	1×32	$1 \times 4.82 \cdot 10^6$
blade	2×40	$2 \times 3.94 \cdot 10^6$
blade "hole"	2×1	-
total	**114**	**$12.70 \cdot 10^6$**

The cylindrical background grid (fig. 4) of a height of 6.1 R and radius equal to 4.0 R ensures that the rotor blades are located, at least, 3.0 R from the farfield. The vicinity of the rotor and its wake is solved with a cuboid structure with uniform volumes ($0.1c \times 0.1c \times 0.1c$) (see fig. 5). No chimera interpolation errors appear due to the increase density of the blade

and background grids.

The blade grid (fig. 6) is C-type in streamwise and H-type in crosswise directions. It spans from the surface 1.2 c in all directions (radial and normal). The non-dimensional distance of the first layer of cells from the solid surface of the blade is of the order of $y^+ = 3$, which is sufficient for resolving the laminar part of the turbulent boundary layer using low-Re turbulence model of LEA k-ω. Figure 7 presents the whole chimera overlapping grid topology of the clean case.
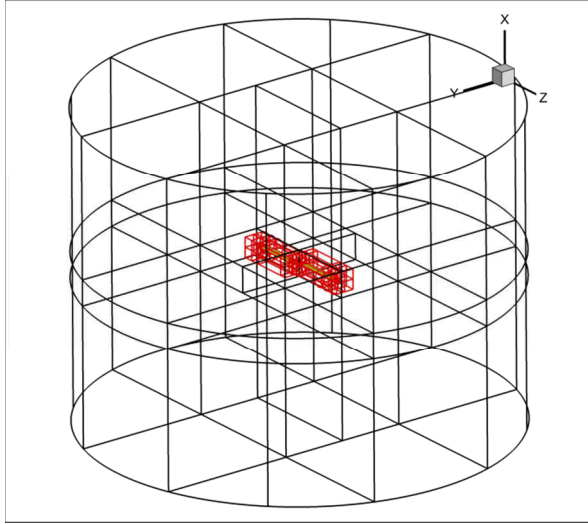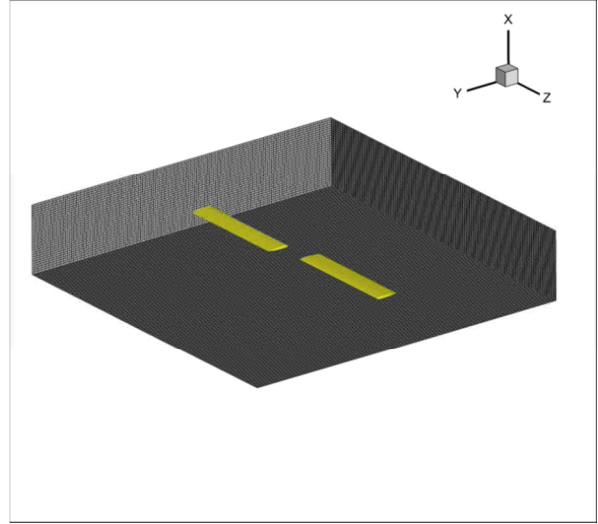

Figure 4: Background component grid

Figure 5: Background component grid – rotor box

Three different boundary conditions are applied in the numerical simulation: no-slip condition with zero heat-flux (adiabatic) applied at the rotor blades, Froude condition at the edges of the background grid (far-field) and special chimera condition at the outer edge of the blade component grids which is necessary for interpolation of the flow value between meshes.
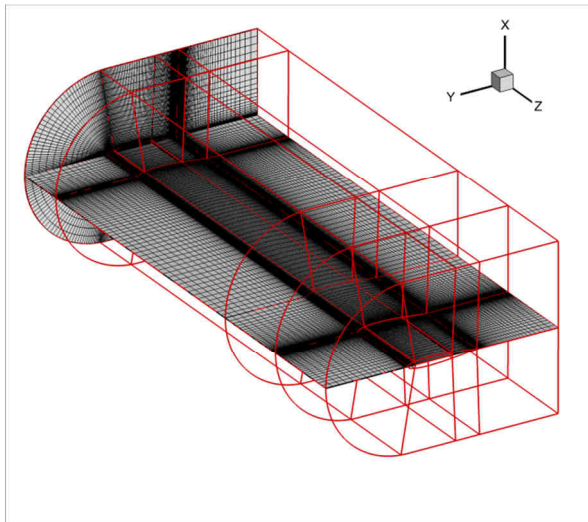

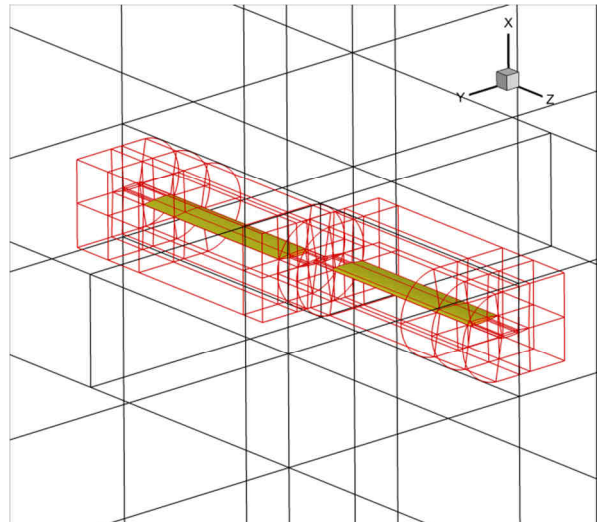**Figure 6**: Blade component grid

Figure 7: Chimera overlapping topology – clean case

The fully-turbulent steady simulation of the flow field around the Caradonna-Tung model rotor overpredicts the experimental thrust coefficient (C_{T-EXP} = 0.00473) by 15% (C_{T-CFD} = 0.00545). Reproducing properly the flow-field around the rotor blades faces with several difficulties. One of them is the properly capture of the rotor wake and the tip vortex path. In the present study, the rotor wake is not set externally but it is a result of the simulation as well. Figure 8 presents the wake structure using Q-criterion and colored by vorticity magnitude revealing contracting and descending helical shape. It is important to remark that an additional refinement of the background chimera component grid would limit the dissipation of the wake.
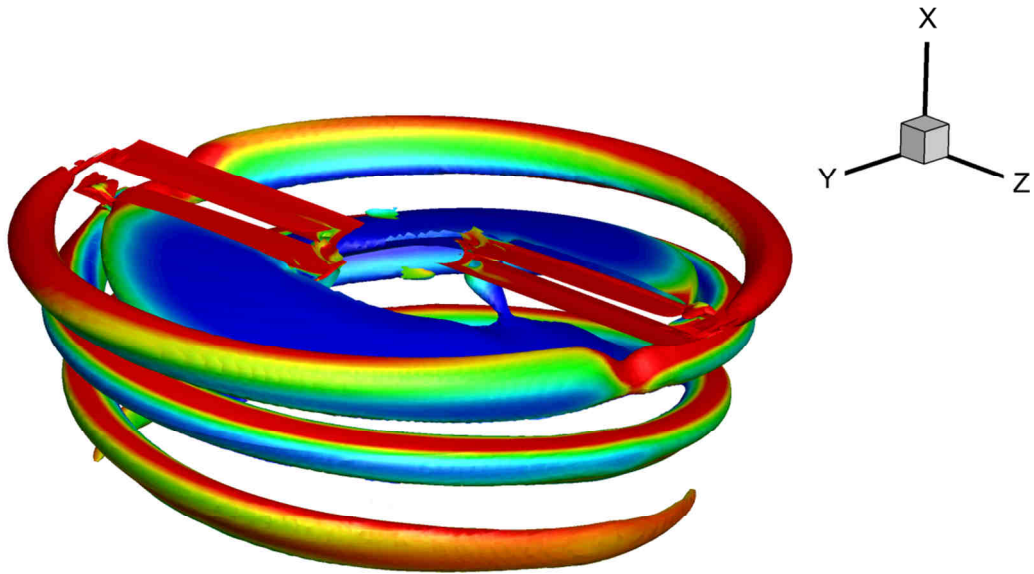

Figure 8: Aerodynamic wake of the Caradonna-Tung rotor

For validation purposes, a comparison of pressure coefficient C_P distributions was performed along the span of the blade (r/R = 0.50, 0.68, 0.80, 0.89, 0.96) and is presented in figure 9. The flow is fully subsonic at the first two cross-sections (r/R = 0.50, 0.68) and supersonic areas terminated by shock waves appear at the remaining sections (r/R = 0.80, 0.89, 0.96). The overall agreement with the experimental data is acceptable.

The acceleration of the flow on the suction side of the blade close to the tip leads to the appearance of strong shock waves which induce flow separation. The pressure distribution and separation bubble size (streamlines in white color) on the suction side of the blade are presented in the figure 9 as well. The extension of the separation bubble in spanwise direction is from r/R = 0.860 to r/R = 0.955. The detachment point is located at x/c = 0.30 and almost constant in radial direction. The reattachment point significantly varies with the cross-section. The most severe reverse flow appears at r/R = 0.92 where the separation bubble length is 15% of the chord.

4.2 Flow control case (RVGs)

Once the numerical model has been validated against experimental data for the clean case, the simulation results can be used for designing the dimensions, number and location of the rods. The diameter, height and spacing are set according to the boundary layer thickness (δ) upstream of the separation bubble.

The boundary layer thickness was calculated based on the comparison of simulated velocity profile and the ideal velocity profile. By imposing constant total pressure P_0 (equal to the value outside of the boundary layer for the clean case), the ideal Mach number (eq. 1) may be calculated and therefore the ideal velocity profile. The boundary layer thickness is defined as the normal distance to the wall at which there is a difference between both profiles of 1% of the ideal one.

$$\frac{P}{P_0} = \left(1 + \frac{\gamma - 1}{2} M^2\right)^{-\frac{\gamma}{\gamma - 1}} \tag{1}$$
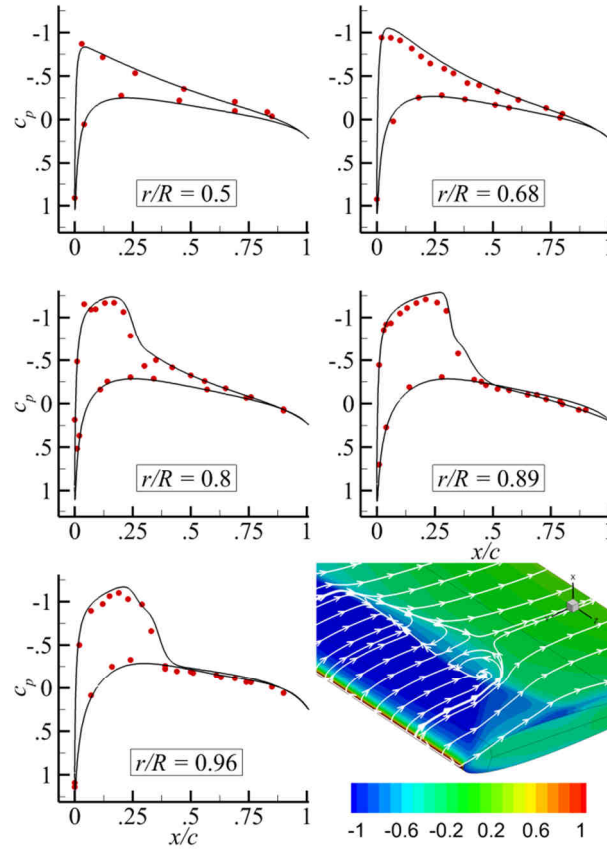

Figure 9: Pressure coefficient (C_P) distribution and separation bubble

For the clean high-speed hover case studied in the present paper, the boundary layer thickness upstream of the shock wave was approximately 0.008 c at x/c = 0.20 (due to the rotor blades were scaled to have a chord equal to 1 meter, the boundary layer thickness was approximately 8 mm). The rod was designed according to previous investigations [2] where it

was concluded that the optimum rod design should keep the following relations: $\phi = \delta\,/4$, $h = \delta\,/2$ and $L = 2.5 \cdot \delta$. Due to large length of the separation bubble in spanwise direction, the spacing between rods was increased to $5 \cdot \delta$ in order to reduce the number of volumes of the RVG component grid (still very computationally demanding). Table 2 summarizes parameters of the designed RVGs.

All together 14 RVGs were placed between r/R = 0.86 and r/R = 0.955 (covering the whole separation bubble in spanwise direction) and at x/c = 0.20. The rods were located $12.5 \cdot \delta$ upstream the flow separation. The optimum location of RVGs on the blade is still under research but it is already known that: they can not be located close to the separation point (there is insufficient space to develop stable vortical structures), nor very far (streamwise vorticity is strongly dissipated) [10].

Table 2: RVG flow control device

Diameter (ϕ)	2 mm
Height (h)	4 mm
Spacing (L)	40 mm
Skew angle (α)	45˚
Pitch angle (Θ)	30˚
number of RVGs	14

For the flow control case, the RVG grid component is added to the project of the previously described clean case chimera set-up. It is placed on the suction side of the blade and spans 0.2 c in radial direction to the tip respect the outer rod, 0.5 c in radial direction to the root respect the inner rod and 0.5 c in normal direction. Figure 10 presents the grid topology for the rod vortex generators placed on the surface of the blade and a detailed view of the rods is presented in figure 11. The chimera overlapping grid topology for the RVG case is showed in figure 12. The complete set of meshes for the RVG case consists of 616 blocks and 36.70 millions of control volumes. Table 3 summarizes the components, number of blocks and number of volumes.
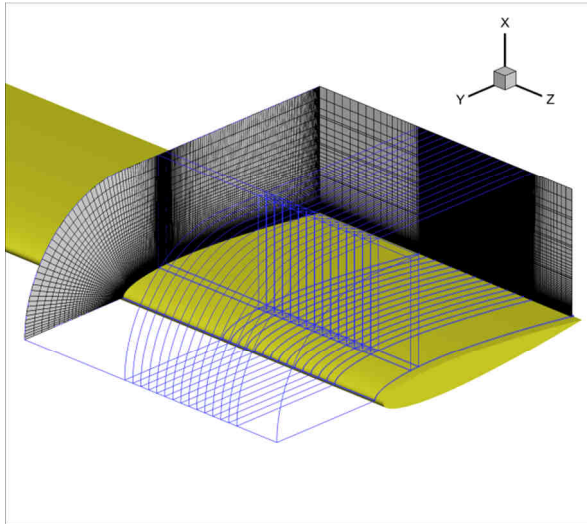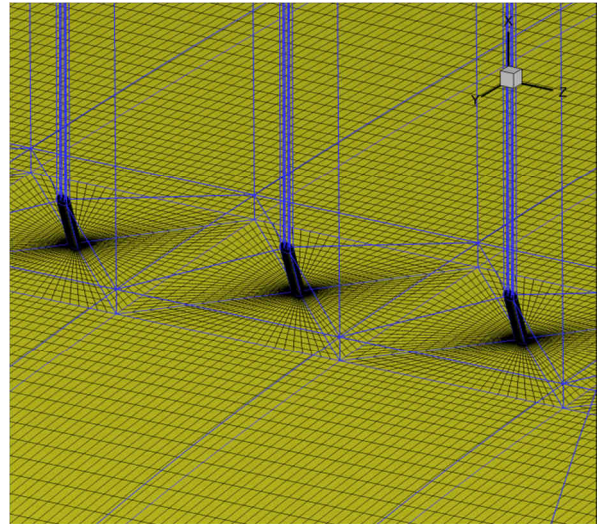

Figure 10: RVG component grid

Figure 11: RVG surface mesh in more details

Table 3: Grid components for the RVGs case

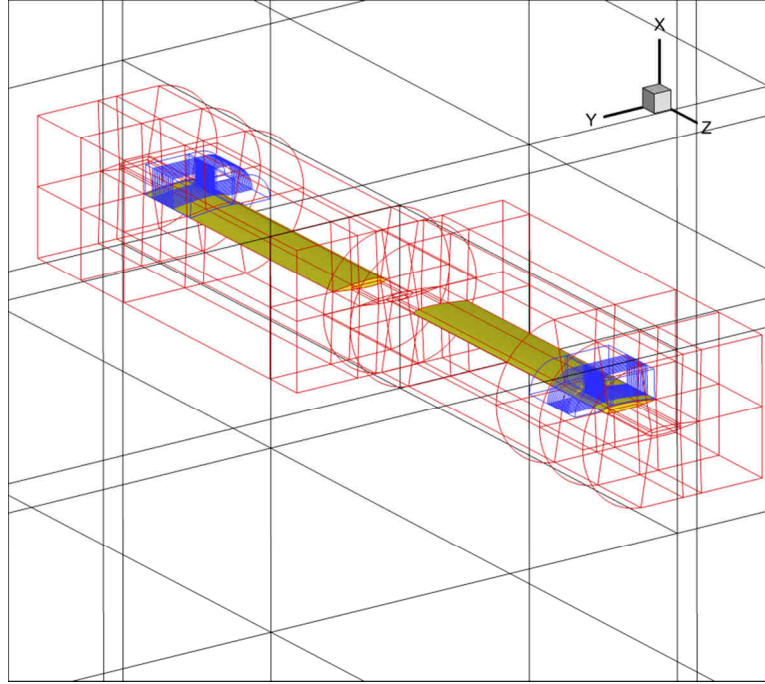| grid component	number of blocks	number of volumes
background	1×32	$1 \times 4.82 \cdot 10^6$
blade	2×40	$2 \times 3.94 \cdot 10^6$
blade "hole"	2×1	-
RVG	2×250	$2 \times 12.00 \cdot 10^6$
RVG "hole"	2×1	-
total	**616**	**$36.70 \cdot 10^6$**

Figure 12: Chimera overlapping grid topology for the RVG case

Figure 13 presents the development of the streamwise vortex in five chordwise sections ($x/c = 0.22, 0.25, 0.27, 0.29, 0.33$). It is worth to mention that the effect of the rods is only visible below the edge of the boundary layer thickness where the vortex generators are submerged. Upstream of the separation bubble ($x/c = 0.22, 0.25, 0.27, 0.29$), the vortex develops increasing the intensity. On the other hand, when the flow separation starts ($x/c = 0.30$), the vortex core is lifted and highly dissipated (see in figure 13 – $x/c = 0.33$). The numerical simulation reveals that there is no sign of any vortex pattern downstream of the reattachment point. The same behaviour was pointed out in previous experimental investigations and numerical simulations of the air jet streamwise vortex generators [11].

The properties of the flow in the boundary layer are changed due to the formation of the streamwise vortex (see fig.14). The flow is attracted towards the blade surface which increases the shear stress. Four chordwise sections ($x/c = 0.25, 0.35, 0.40, 0.60$) are presented in figure 14 for two different radial sections: $r/R = 0.911$ and $r/R = 0.922$. The first station of $r/R = 0.911$ is located between rods (where the flow control device is expected to have minor influence on the mean flow), while $r/R = 0.922$ is located directly in the wake of the RVG

8

with a maximum influence on the flow. For the first chordwise location of x/c = 0.25, the boundary layer profile is more full for the flow control case compared to clean case at r/R = 0.922. On the other hand, the boundary layer properties in the other radial section are almost constant and not influenced by streamwise vorticity. Travelling downstream (x/c = 0.35), the flow separation appears in the clean case but the flow is attached for the RVG case in both radial sections making the boundary layer profiles fuller. The other positive effect of the flow control may be observed at x/c = 0.40. Although the flow is not attached at r/R = 0.922, the height of the separation bubble is reduced. The comparison makes evident that not only the area of projection of the separation bubble on the surface is reduced but also the height of the bubble. Lastly, when the flow reattaches to the blade at x/c = 0.60, the boundary layers are similar.
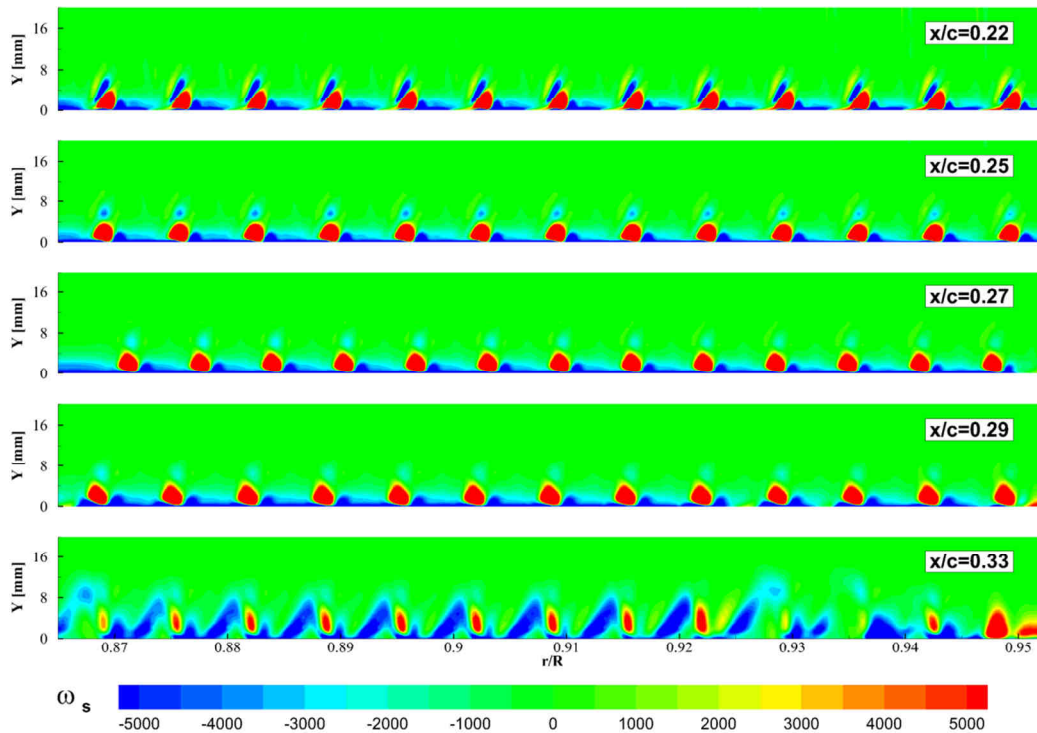

Figure 13: Streamwise vortex development in space

The numerical results of the flow past the rotor blade with the proposed passive flow control system reveal the possibility of elimination of separation bubble (fig. 15). The figure presents the contour map of friction coefficient and the location of the separation bubble. The use of rod vortex generators leads to an increase of the skin friction and reduction of separation area. The bubble is not completely eliminated but it is divided into smaller ones. For this reason, the full elimination of the reverse flow may be obtained by two different approaches: either increase the diameter and/or height of the rods (increased streamwise vortex strength) or decrease spacing between the rods (more influence in the spanwise direction).
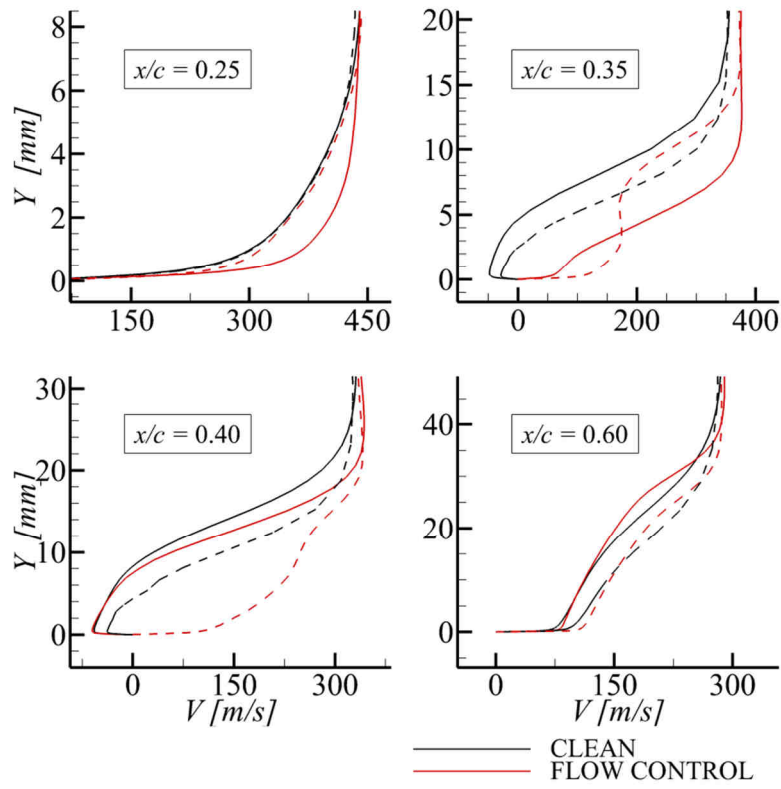
Figure 14: The effect of RVGs on the boundary layer development. Dashed line for r/R = 0.911 and solid line for r/R = 0.922
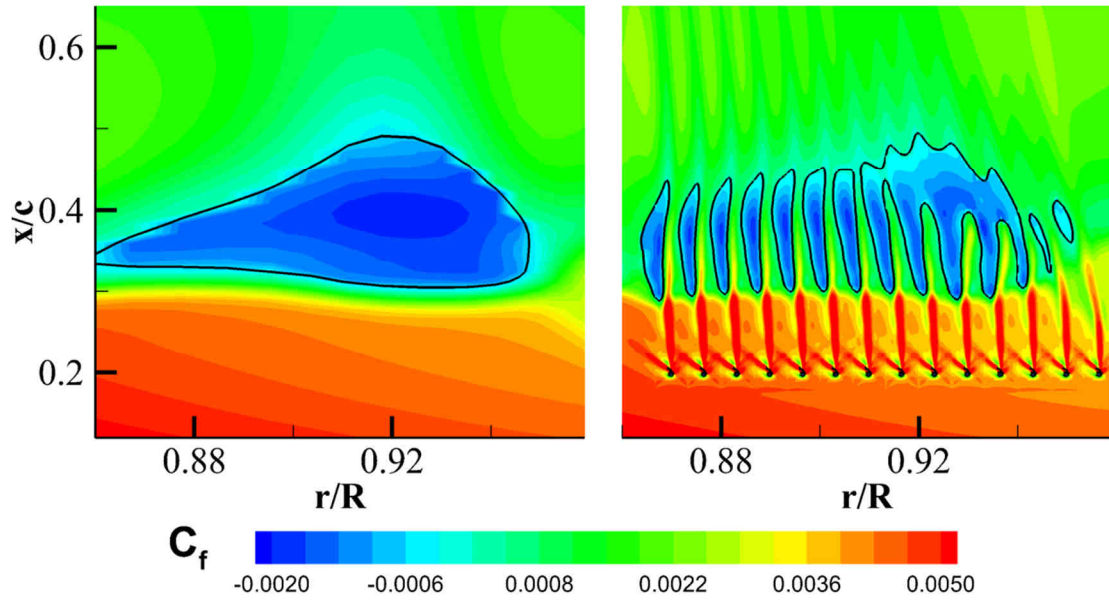

Figure 15: The effect of RVGs on the size of the separation bubble and wall shear stress (friction coefficient)

10

The numerical simulation provides a thrust coefficient equal to $C_{T\_CFD\_RVG} = 0.00557$. The use of RVGs on the blades of the Caradonna-Tung model helicopter rotor improves the thrust by 2.2% in respect to the clean case. It is important to mention that more severe conditions (higher collective or rotational speed) would induce stronger flow separation and the flow control system would be more effective [10]. The use of rod vortex generators increases the power consumption by 1.2% respect the clean case ($C_{P\_CFD\_RVG} = 0.000630$ against $C_{P\_CFD\_CLEAN} = 0.000623$). The use of RVGs induces a parasitic drag which needs to be compensated with more power consumption. Although this effect is a drawback of the proposed flow control, overall the performance of the helicopter rotor is improved ($C_{T\_c}/C_{P\_c} = 8.75$ for the clean case against $C_{T\_r}/C_{P\_r} = 8.84$ for the flow control case).

5 CONCLUSIONS

It has been proven that the numerical model implemented in FLOWer code is able to reproduce the main features measured in the experiments for the clean case. The appearance of flow separation suggested the possibility of application of a flow control device for improving the aerodynamic performance of the rotor. The numerical results related to the implementation of rod vortex generators on hovering helicopter rotor blades confirm that this method of passive control reduces the flow separation increasing thrust over power consumption. In the next step, a high-speed forward flight case with rod vortex generators will be analyzed.

REFERENCES

[1] Patent application P.389685, *Streamwise vortex generator,* Poland.
[2] Doerffer, P., UFAST: Experiments Data Bank: Unsteady effects of shock wave induced separation. ISBN 978-83-88237-47-1, 2009.
[3] Rossow, C.-C., Kroll, N. and Schwamborn, D. The MEGAFLOW project − numerical flow simulation for aircraft. In: Di Bucchianico, A., Mattheij, R. M. M., Peletier, M. A. (eds.), *Progress in Industrial Mathematics at ECMI 2004*, vol. 8, pp. 3-33, Springer, 2006.
[4] Caradonna, F.X., Tung, C.: Experimental and analytical studies of a model helicopter rotor in hover. *NASA Technical Memorandum 81232*, 1981.
[5] Schwarz, T. The overlapping grid technique for the time accurate simulation of rotorcraft flows. *Proceedings of the 31st European Rotorcraft Forum*, Florence, Italy, 2005.
[6] Rung, T., Lübcke, H., Franke, M., Xue, L., Thiele, F. and Fu, S. Assessment of explicit algebraic stress models in transonic flows. *Proceedings of the 4th International Symposium on Engineering Turbulence Modelling and Measurements*, Ajaccio, France, 1999.

[7] Doerffer, P., Szulc O.: Numerical Simulation of Model Helicopter Rotor in Hover. *TASK Quaterly*, vol. 12, no. 3, 2008.

[8] Doerffer P., Szulc O., Tejero E., F. L., Martinez S., J.: Aerodynamic and Aero-acoustic Analysis of Helicopter Rotor Blades in Hover. In: Bubak, M., (ed.), *E-science on Distributed Computing Infrastructure: PLGrid Plus*, LNCS, Springer, 2014

[9] Doerffer, P., Tejero E., F. L., Szulc, O.: Numerical Simulation of Model Helicopter Rotor in Hover using Chimera Overlapping Grids Technique*, IMP PAN Report No. 29/2014*, Institute of Fluid-Flow Machinery, Poland, 2014

[10] Tejero E., F. L., Doerffer, P., Szulc, O.: Effect of Passive Air Jet Vortex Generator on NACA0012 Performance*, Proceedings of the 5th European Conference for Aerospace Sciences*, Munich, Germany, 2013.

[11] Tejero E., F. L., Doerffer, P.: Numerical Investigation of Flow Separation Using Air Jet Vortex Generators on NACA0012 for Transonic Conditions*, Proceedings of the Congress on Numerical Methods in Engineering*, Bilbao, Spain, 2013.